Anexo B

VERIFICATION OF THE MM5 MODEL USING RADIOSONDE DATA FROM MADRID-BARAJAS AIRPORT

Posada, R.[a,*], García-Ortega, E.[a], Sánchez, J. L.[a], López, L.[a]

[a] *University of León, Spain*

Abstract

Vertical profiles of temperature, water vapor and wind field were traditionally obtained from radiosonde observations for the analysis of mesoscale phenomena. The scarce amount of radiosonde data available and the inadequate temporal and spatial resolution, motivated the development of prognostic soundings derived from Numerical Weather Prediction (NWP) models. Their use should be subject to previous quality verification of model outputs. This work is focused on the evaluation of the NCAR/Penn State Fifth Generation Mesoscale Model MM5 outputs under snow precipitation conditions in the Sierra de Guadarrama (Madrid). A comparison of forecasted vertical profiles of temperature, water vapor density and wind field with those observed by the Madrid- Barajas Airport rawinsonde was carried out. The results showed that the MM5 vertical profiles were able to represent thermodynamic conditions during winter precipitation events. Correlation coefficients of temperature and water vapor were close to 1 at both times. Wind field forecast was also accurate since wind direction and wind speed correlation coefficients were statistically significant for a 95% confidence. It was also found that MM5 simulations remained accurate after 24 h from the initialization.

Keywords: ground-based microwave radiometer; temperature and humidity profiles; continuous measuring; radiosonde sounding

[*] Corresponding author: Group for Atmospheric Physics, Instituto de Medio Ambiente
Email address: rposn@unileon.es (Posada, R.)

1. Introduction

The thermodynamic state of the atmosphere has been studied traditionally from radiosonde data, which provide information about vertical profiles of temperature, water vapor, and wind speed and direction. For decades, analysis of severe phenomena has been based on the study of sounding data (e.g. Davies, 2004; Fawbush and Miller, 1952; Maddox, 1976; Pascual et al. 2012; Rasmussen and Blanchard, 1998, Sánchez et al., 2001; Thompson et al., 2003) which requires the selection of a set of proximity criteria that provide a representative sampling of the meteorological conditions of the study area. The uncertainty of the spatial and temporal scales of the mesoscale phenomena, led to a great variability of the proximity criteria used (Potvin et al., 2010). For instance, for severe convection events, Thompson et al. (2003) defined a maximum distance of 40 km away from the location of the event, and within 30 minutes before or after its formation. However, Rasmussen and Blanchard (1998) considered representative radiosondes to be those that were launched up to 400 km away from the event, and within 3 hours before and 6 hours after its formation. Furthermore, Tudurí et al. (2003) showed that proximity soundings should be defined, not only in terms of distance and time, but also including some geographical and dynamic aspects. Another restriction of radiosondes are their limited temporal resolution -usually launched only two times a day- and their low spatial distribution in some areas of the world, such as the Mediterranean basin (Romero et al. 2007).

These limitations have motivated the development of prognostic radiosondes provided by Numerical Weather Prediction (NWP) models (Hamil and Church, 2000; Hart and Forbes; 1999; Hart et al., 1998; Niziol and Mahoney, 1997). Hamill and Church (2000) found that the Rapid Update Cycle (RUC) model was capable of producing prognostic soundings which could be used to discriminate between meteorological environments that support thunderstorms of varying intensities. Lee (2002) used the reanalysis data provided by the National Centers for Environmental Prediction (NCEP) (Kalnay et al., 1996) to obtain "pseudo-proximity" soundings that were able to produce vertical profiles similar to those derived from observed radiosonde data. More recently, Brimelow et al. (2006), revealed the feasibility of using prognostic soundings from the Global Environmental Multiscale (GEM)

model to assist in forecasting the occurrence of hail over the Canadian prairies.

The higher horizontal resolution of the numerical model forecasts compared to the observed sounding network is attractive for studying mesoscale phenomena (Brooks et al., 2003). However, prior to using NWP models for retrieving prognostic soundings, it is necessary to verify the quality of their outputs, which are dependent on the parameterization schemes selected (Fita, 2008).

A project carried out during winter campaigns in the Sierra de Guadarrama (Madrid) gave us the opportunity to run the NCAR/Penn State Fifth Generation Mesoscale Model MM5 (Grell et al., 1994) with high vertical (65 vertical levels) and horizontal resolutions (3.3 km in the inner domain) for snow precipitation events. This paper is focused on the evaluation of the MM5 outputs, done by comparing atmospheric vertical profiles of temperature, humidity and wind speed and direction with those observed by radiosounding data at the Madrid-Barajas Airport. A high accuracy level between forecasted and observed data would allow us to use predicted profiles of temperature, water vapor and wind speed and direction as proximity soundings for studying, at least, snow precipitation episodes. In addition, other mesoscale phenomena such as internal gravity waves, whose formation is basically dependent on static stability and wind flow, can be studied using the MM5 outputs.

2. Data and methodology

A total of 87 days of snow precipitation recorded in the Sierra de Guadarrama (Madrid) were used to verify the model. The unique observational data available in the vicinity of the study were those collected by the rawinsonde launched from the Madrid-Barajas Airport (40º 30' 36" N, 3º 34' 3" W) two times a day: at 0000 and 1200 UTC. The balloons, operated by the National Agency of Meteorology (Agencia Estatal de Meteorología, AEMET) were equipped with the Vaisala rawinsonde RS92-SGP. In relation to the numerical model used, three nested 100×100 grid domains using Lambert's conformal projection were set up to obtain the highest resolution over the area of interest (Fig. 1). The domains had a horizontal resolution of 30, 10 and 3.3 km, respectively. The vertical resolution was of 65

sigma levels, and the initial conditions were constructed from reanalysis data of the NCEP, with a 1.0^{o} resolution available at 0000, 0600, 1200 and 1800 UTC. The temporal resolution of the outputs was of 6 h for the first domain, 3 h for the second, and 1 h for the third one. The duration of each run was of 24 h, starting at 0000 UTC. The model used the Reisner Graupel microphysics scheme (Reisner et al., 1998), which takes into account the graupel and ice concentration in the atmosphere; the ETA boundary layer scheme, the Kain-Fritsch 2 cumulus parameterization (Kain, 2004) for domains 1 and 2 (explicit physics was used for the inner domain), and the cloud radiation scheme (Stephens, 1984; Stephens, 1978; Garand, 1983). The verification for the thermodynamic variables of temperature, water vapor density and wind speed and direction was carried out. A period of 12 h was considered in order to stabilize the model outputs. Therefore, the comparison was done with the soundings launched at 1200 and 0000 UTC the next day (D+1). Since sounding balloons move vertically and horizontally, in accordance with wind speed and direction (Kitchen, 1989, McGrath et al., 2006), it was established to work with the mean profile of a 33×33 km grid (10×10 grid points of similar height) centered in Madrid-Barajas Airport. Additionaly, due to the different vertical resolutions (the model provides fixed levels for pressure, while the radiosonde provides varying vertical variables), and to avoid errors associated with interpolations, data corresponding to different heights inferior to ±50 m were used.

To quantify the accuracy of the forecast, several standard statistical parameters were carried out: the bias, the root mean squared error (rmse) and the standard deviation (σ).

3. Results

3.1. Verification of vertical temperature profiles

The dispersion diagrams in Fig. 2 represent the comparison of vertical temperature profiles predicted by MM5 simulations with the radiosonde observations at 1200 UTC (Fig. 2a) and at 0000 UTC (D+1) (Fig. 2b). A high correlation coefficient ($\sim$1) was observed between temperature forecasted and observed at both hours, although the rmse increased slightly, from 1.7 ^{o}C at 1200 UTC to 1.8 ^{o}C at

0000 UTC (D+1). The bias, however, did not differ much, since it was around 0.4 ^{o}C in both cases.

By levels (Fig. 3a), the correlation coefficient was statistically significant at every interval for a 95% confidence, except between 9500 and 10000 m at 1200 UTC, and between 10500 and 11000 m at 0000 UTC (D+1). In both cases, the low correlation was due to the small sample size compared (4 and 3 cases, respectively). The maximum error made by the model with regard to the soundings was 2.5 ^{o}C between 5500-6000 m. Apart from that, the model tended to overestimate the temperature at most levels, with a mean bias of 0.6 ^{o}C (Fig. 2c). At 0000 UTC (D+1) the highest rmse was found at 4000-4500 m, with a value of 2.5 ^{o}C. The standard deviation of the MM5 was very similar to that of the sounding at 1200 and at 0000 UTC (D+1) (Fig. 2d).

3.2. Verification of vertical water vapor density profiles

The dispersion diagrams (Fig. 4a and Fig. 4b) show that prognostic humidity had a correlation of 0.98 with observed humidity, at both hours (1200 and 0000 UTC (D+1)). The MM5 rmse was 0.4 g m^{-3} at 1200 UTC, and 0.5 g m^{-3} at 0000 UTC (D+1). The bias was approximately 0.2 g m^{-3}, although it was slightly higher at 0000 UTC (D+1). By levels (Fig. 3b), it is of interest that the correlation coefficient is statistically significant, for a 95% confidence, up to 9500 m at 1200 UTC. Over this level, the water vapor content was almost zero and, in these cases, the correlation factor is very sensitive to small variations. The rmse and bias presented low values, although the bias indicated an overestimation of water vapor content at every level. At 0000 UTC (D+1) the results were very similar. However, the correlation was not significant over 8000 m. The model overestimated the water vapor content at every interval (Fig. 4d).

3.3. Verification of vertical wind speed and direction profiles

For the case of wind field, the observed and/or modeled wind speeds of 0 m s^{-1} were removed from the database, since in those cases the direction angle (α) is undefined. For this reason, the sample size at 1200 UTC was reduced from 1020 to 1012 cases. The results of the verification showed that, at 1200 UTC (Fig. 5a),

prognostic wind had a statistically significant correlation coefficient (0.96), with a confidence of 95%. The bias was 0.3 m s^{-1} and the rmse 4.2 m s^{-1}. At 0000 UTC (D+1) (Fig. 5b) the correlation was also high (0.95) and, although the rmse increased up to 4.5 m s^{-1}, the bias was below 0.1 m s^{-1}.

In regard to the levels (Fig. 3c), the wind speed correlation at 1200 UTC was statistically significant at every interval. Between the ground and 200 m, the correlation was lower than at higher levels, where the correlation reached values close to 1. Between the ground and 4000 m, the model overestimated the wind speed with a maximum of 1.7 m s^{-1} over the observed value. Between 4000 and 7000 m, there was not a clear tendency of the bias, but at heights over 7000 m, the model tended to underestimate wind speed. The highest negative bias was found between 11000 and 12000 m, and the rmse ranged between 2.5 m s^{-1} (ground-1000 m) and 5.4 m s^{-1} (10000-10500 m) (Fig. 5c).

At 0000 UTC (D+1) the wind speed correlation was statistically significant at every level, except between 9500 and 10000 m, and 10500 and 11000 m. At this layer, the correlation was negative; due to the small sample size (it was only possible to compare 3 cases). Broadly speaking, the correlation degraded compared to the correlation at 1200 UTC, especially at the highest levels. The rmse also increased, ranging from 2.5 m s^{-1} (ground-1000 m) and 6.9 m s^{-1} (7500-8000 m) [1] (Fig. 5d).

In regard to wind direction, Fig. 6a-b shows that most of the winter precipitation events were produced under situations with SW and NW flow, which is in accordance with the estimation made by the model (Fig. 6c-d).

The same result is shown in the dispersion diagrams of direction angles (Fig. 7a-b). These figures are not appropriate when comparing angles close to 0º with others around 360o, since it produces a low correlation coefficient that does not correspond to the actual correlation. To diminish this limitation, the method employed by Risch and Eastham (2011) was applied: if the difference between the model angle (α_{MM5}) and the sounding angle (α_{RW}) was lower than 45º, and one

[1] The MM5 rmse produced at the 10500-11000 layer (10.3 m s^{-1}), is not representative since the sample size is very small (3 pairs of values compared).

of them had a value slightly below 360o and the other one slightly over 0º, 360º were added to the angle of lower value. Thus, a new angle was defined ($\alpha\prime$), which was equivalent to the original. This caused the angle range to be extended to 405º. Most values, at 1200 and 0000 UTC (D+1), were concentrated in the NW and SW quadrants, and had very high correlation coefficients at both hours (0.94 and 0.92, respectively). The correlation was also high and statistically significant at every level (Fig. 3d). The bias was around 0º in all cases. (Fig. 7c-d).

To complete the wind direction verification, a histogram of angle differences was done. In this manner, it could be possible to evaluate the angular difference between prognostic wind and observed wind. At 1200 UTC (Fig. 8a) it was seen that 33.8% of the sample presented an angle difference of $\pm$10º, and 95% was below $\pm$50º. At 0000 UTC (D+1), the case with a difference of $\pm$10º decreased to 30.9%, but 95% of the sample remained below $\pm$50º (Fig. 8b).

4. Discussion

In this paper a verification of the MM5 outputs of temperature, water vapor density and wind field was done. In order to do so, the outputs were compared with the Madrid- Barajas Airport sounding observations. The results showed that the MM5 experiments designed were capable of producing realistic prognostic soundings during winter precipitation events. Temperature profiles and absolute humidity are in very similar to those measured by radiosoundings, since the correlation coefficients were close to 1. Furthermore, it was found that wind field was also modeled properly, since the correlation coefficient for predicted wind speed was statistically significant at all heights for a 95% confidence level. With regard to wind direction, correlation coefficients were 0.94 at 1200 UTC, and 0.93 at 0000 UTC (D+1), although low correlations were found when comparing angles close to 360º and to 0º. To determine the actual difference between observed and forecast wind direction, an angular difference was carried out (α_{RW}-α_{MM5}). It showed that 95% of modeled wind direction did not differ more than $\pm$50º with regard to observed direction angles. At 0000 UTC (D+1), the results were similar to those found at 1200 UTC, meaning that the MM5 forecast remained accurate 24 hours after model initialization. Therefore, the MM5 simulations here mentioned are a

good tool for retrieving prognostic soundings of temperature, humidity, and wind speed and direction. They can be used as proximity soundings for the study of several mesoscale phenomena with a high degree of confidence, including those mainly dependent on air flow, such as internal gravity waves.

References

[1] Brimelow, J. C., G. W. Reuter, R. Goodson, T. W. Krauss, 2006. Spatial forecasts of maximum hail size using prognostic model soundings and HAILCAST. Wea. Forecast., 21, 206-219.

[2] Brooks, H. E., J. W. Lee, J. P. Craven, 2003. The spatial distribution of severe thunderstorm and tornado environments from global reanalysis data. Atmos. Res., 67-68, 73-94.

[3] Davies, J. M., 2004. Estimations of CIN and LFC associated with tornadic and nontornadic supercells. Wea. Forecast. 19, 714-726.

[4] Fawbush, E., R. Miller, 1952. A mean sounding representative of the tornadic airmass environment. Bull. Amer. Meteor. Soc. 33, 303-307.

[5] Fita, L., 2008: Numerical study of intense cyclogenesis events in the Mediterranean basin. Ph.D. dissertation, Universitat de les Illes Balears.

[6] Garand, L., 1983. Some improvements and complements to the infrared emissivity algorithm including a parameterization of the absorption in the continuum region. J. Atmos. Sci., 40, 230-243.

[7] Grell, G. A., J. Dudhia, D. R. Stauffer, 1994. A description of the fifth-generation Penn State/NCAR mesoscale model (MM5). NCAR Technical Note, NCAR TN-298 +STR, pp. 121.

[8] Hamill, T. M., A. T. Church, 2000. Conditional probabilities of significant tornadoes from RUC-2 forecasts. Wea. Forecast., 15, 461-475.

[9] Hart, R. E., G. S. Forbes, 1999. The use of hourly model-generated soundings to forecast mesoscale phenomena. Part II: Initial assessment in forecasting nonconvective strong wind gusts. Wea. Forecast. 14, 461-469.

[10] Hart, R. E., G. S. Forbes, R. H. Grumm, 1998. The use of hourly model-generated soundings to forecast Mesoscale phenomena. Part I: Initial assessment in forecasting warm-season phenomena. Wea. Forecast. 13, 1165-1185.

[11] Kain, J. S., 2004. The Kain-Fritsch Convective Parameterization: An Update. J. Appl. Meteor. 43, 170-181.

[12] Kalnay, E. et al., 1996: The NCEP/NCAR 40-year reanalysis project. Bull. Amer. Meteor. Soc., 77, 437-470.

[13] Kitchen, M., 1989. Representativeness errors for radiosonde observations. Q. J. R. Meteorol. Soc. 115, 673-700.

[14] Lee, J. W., 2002: Tornado Proximity Soundings from the NCEP/NCAR Reanalysis Data. Ph.D. dissertation, University of Oklahoma.

[15] Maddox, R. A., 1976. An evaluation of tornado proximity wind and stability data. Mon. Weather Rev. 104, 133-142.

[16] McGrath, R., T. Semmler, C. Sweeney, S. Wang, 2006. Impact of balloon drift errors in radiosonde data on climate statistics. Amer. Meteor. Soc. 19, 3430-3442.

[17] Niziol, T. A., E. A. Mahoney, 1997. The use of high resolution hourly forecast soundings for the prediction of lake effect snow. 13th Int. Conf. on Interactive Information and Processing Systems for Meteorology, Oceanography, and Hydrology, Long Beach, California, Amer. Meteor. Soc. 92-95.

[18] Pascual, A., F. Valero, M. L. Martín, A. Morata, M. Y. Luna, 2012. Probabilistic and deterministic results of the ANPAF analog model for Spanish wind field estimations. Atmos. Res., 108, 39-56.

[19] Potvin, C. K., K. L. Elmore, S. J. Weiss, 2010. Assessing the impacts of proximity sounding criteria on the climatology of significant tornado environments. Wea. Forecast., 25, 921-930.

[20] Rasmussen, E. N., D. O. Blanchard, 1998. A baseline climatology of sounding-derived supercell and tornado forecast parameters. Wea. Forecast. 13, 1148-1164.

[21] Reisner, J., R. M. Rasmussen, R. T. Bruintjes, 1998. Explicit forecasting of supercooled liquid water in winter storms using the MM5 mesoscale model. Q. J. R. Meteorol. Soc., 124, 1071-1107.

[22] Risch, C., E. Eastham, 2011. Correlation of Sodar and Met Tower Measurements. CBER Technical Report. Marshall University for Western Virginia Division of Energy, pp. 15. Available online at: $http$: $//www.wvcommerce.org/App_Media/assets/doc/energy/MU_SODAR-Met_Correlation_Report_for_web_April_2011.pdf [Last accessed$: $10/05/2012]$.

[23] Romero, R., M. Gayà, C. A. Doswell III, 2007. European climatology of severe convective storm environmental parameters: A test for significant tornado events. Atmos. Res., 83, 389-404.

[24] Sánchez, J. L.; J. L. Marcos; E. García-Ortega, 2001. Construction and Assessment of a Logistic Regression Model Applied to Short Term Forecast of Thunderstorms in Leon (Spain). Atmos. Res. 56, 57-71.

[25] Stephens, G. L., 1984. The parameterization of radiation for numerical weather prediction and climate models. Mon. Wea. Rev. 112, 826-867.

[26] Stephens, G. L., 1978. Radiation profiles in extended water clouds II: Parameterization schemes. J. Atmos. Sci. 35, 2123-2132.

[27] Thompson, R. L., R. Edwards, J. A. Hart, K. L. Elmore, P. Markowski, 2003. Close proximity soundings within supercell environments obtained from the Rapid Update Cycle. Wea. Forecast. 18, 1243-1261.

[28] Tudurí, E., R. Romero, L. López, E. García, J. L. Sánchez, C. Ramis, 2003. The 14 July 2001 hailstorm in northeastern Spain: Diagnosis of the meteorological situation. Atmos. Res. 67-68, 541-558.

List of Figures

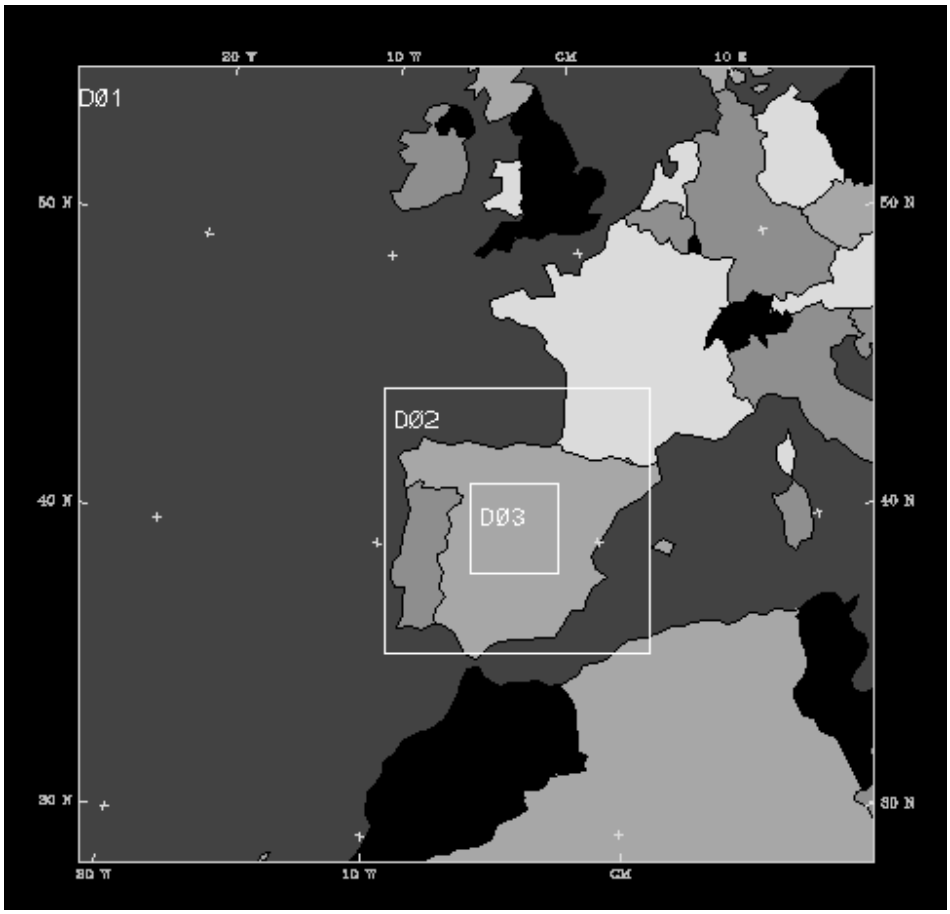

Figure 1: The three nested domains of the MM5 simulations

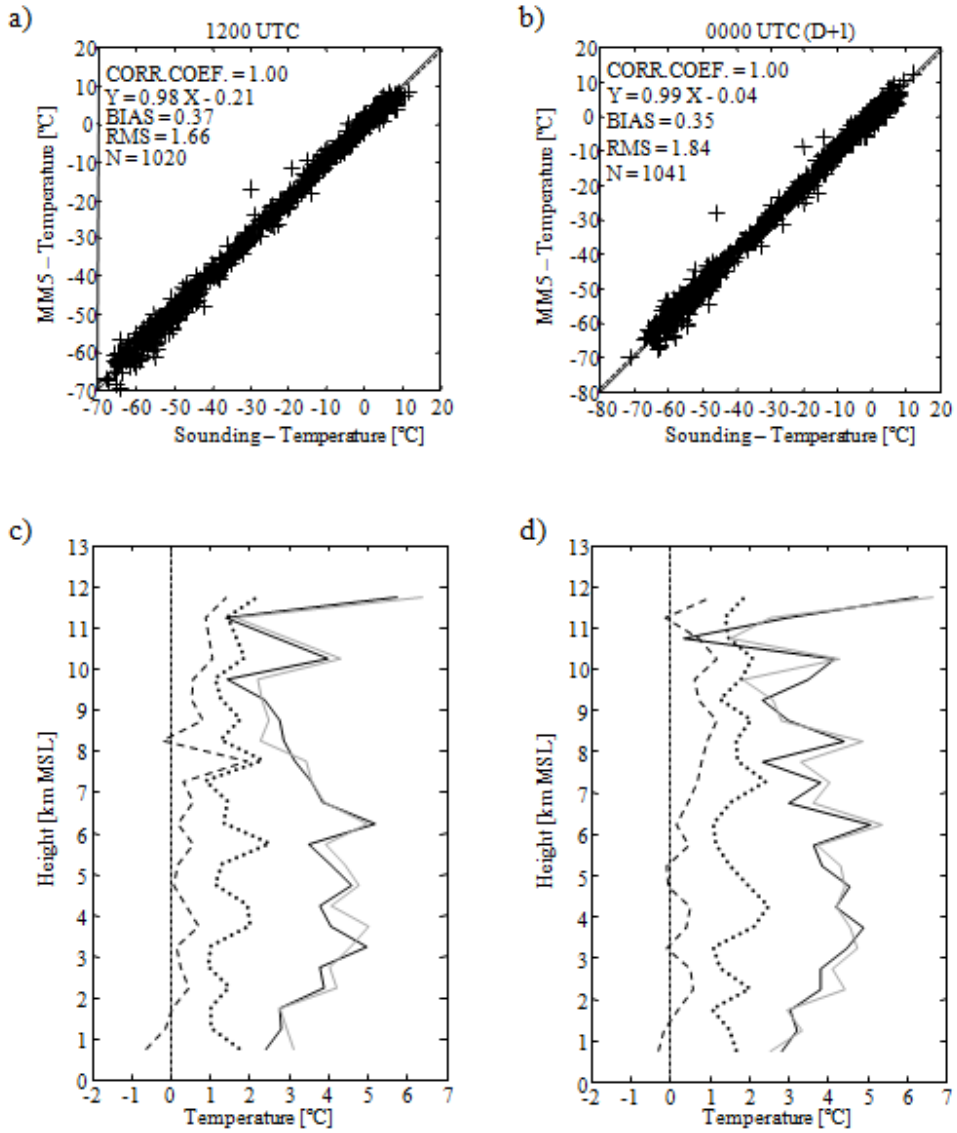

Figure 2: Top: Dispersion diagrams of temperature (a) at 1200 UTC and (b) at 0000 UTC (D+1). The dotted line represents the regression line, and the solid line represents perfect correlation (1:1) between the MM5 and the radiosonde. Bottom: MM5 bias - dashed black line-, MM5 rmse -dotted black line-, MM5 standard deviation -solid black line-, and radiosonde standard deviation -solid grey line-; (c) at 1200 UTC and (d) at 0000 UTC (D+1).

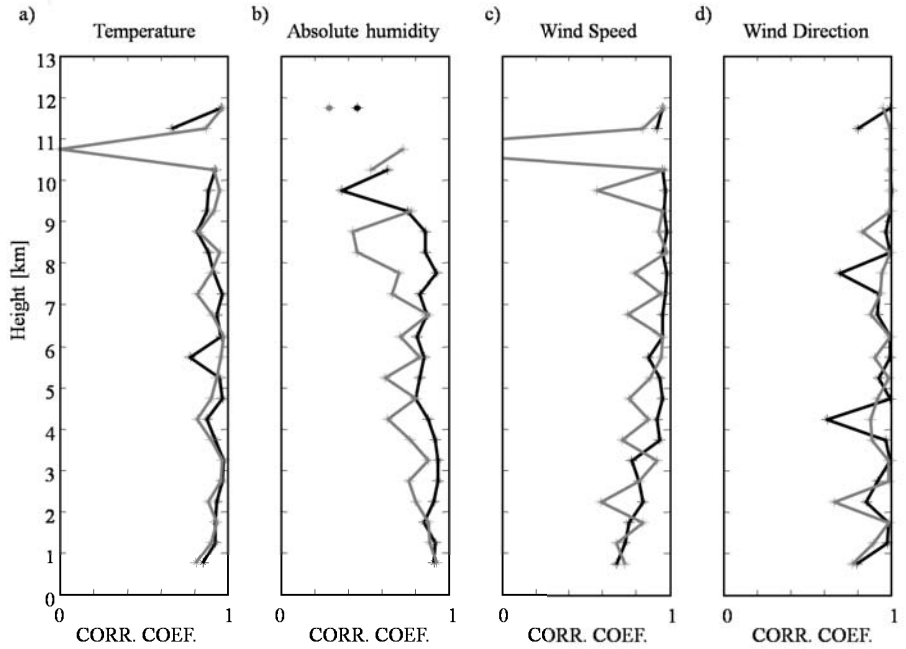

Figure 3: Vertical profiles of correlation coefficients for (a) temperature, (b) absolute humidity, (c) wind velocity and (d) wind direction at 1200 UTC -black line- and 0000 UTC (D+1) -grey line-.

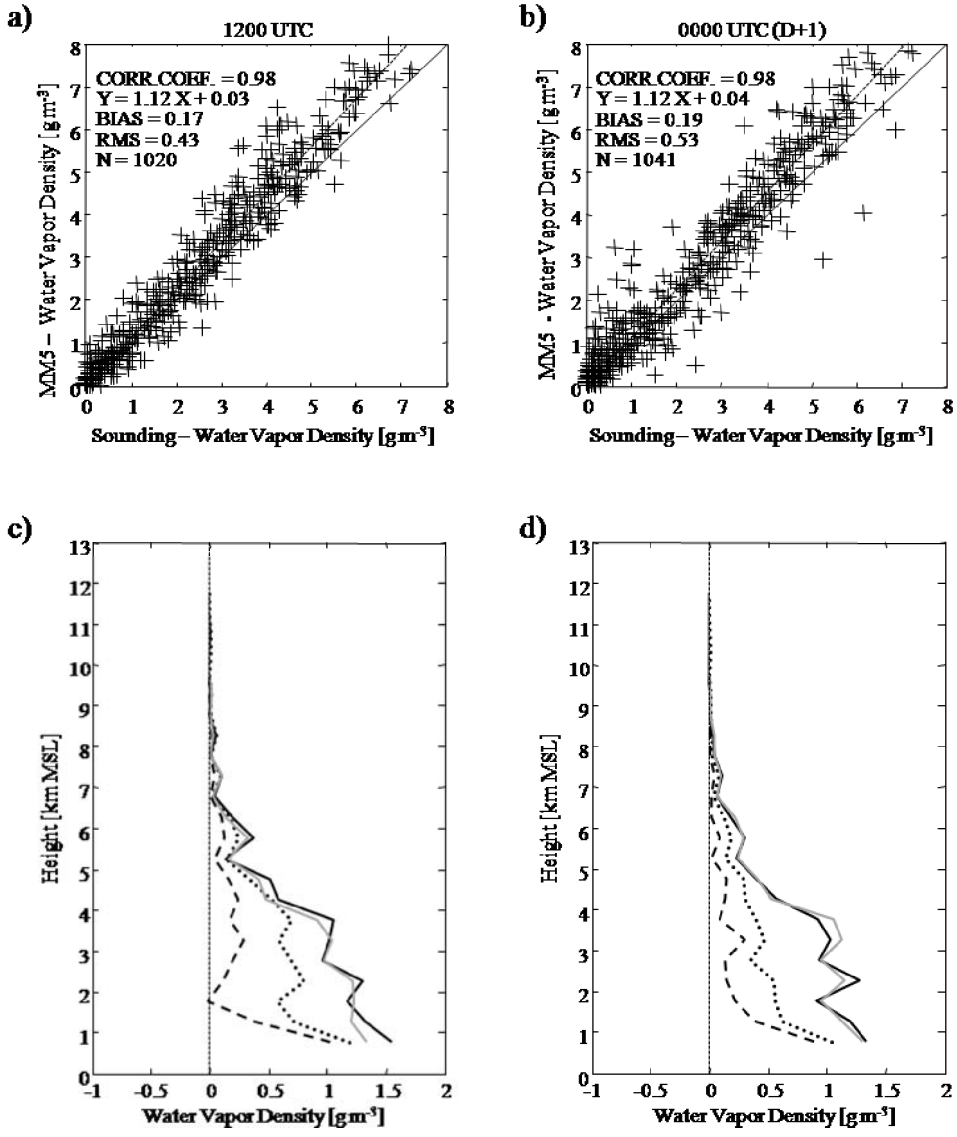

Figure 4: The same as Fig. 2, but for water vapor density.

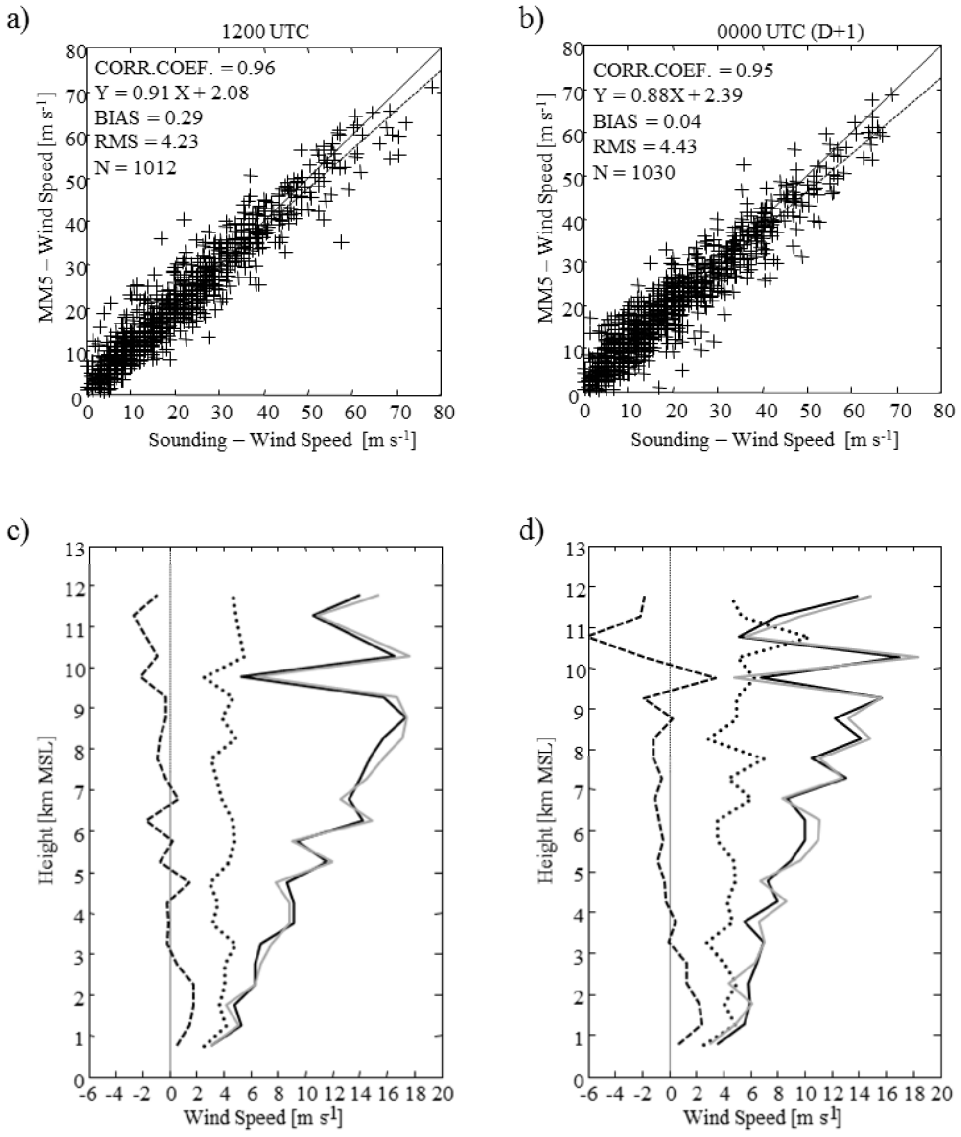

Figure 5: The same as Fig. 2, but for wind speed.

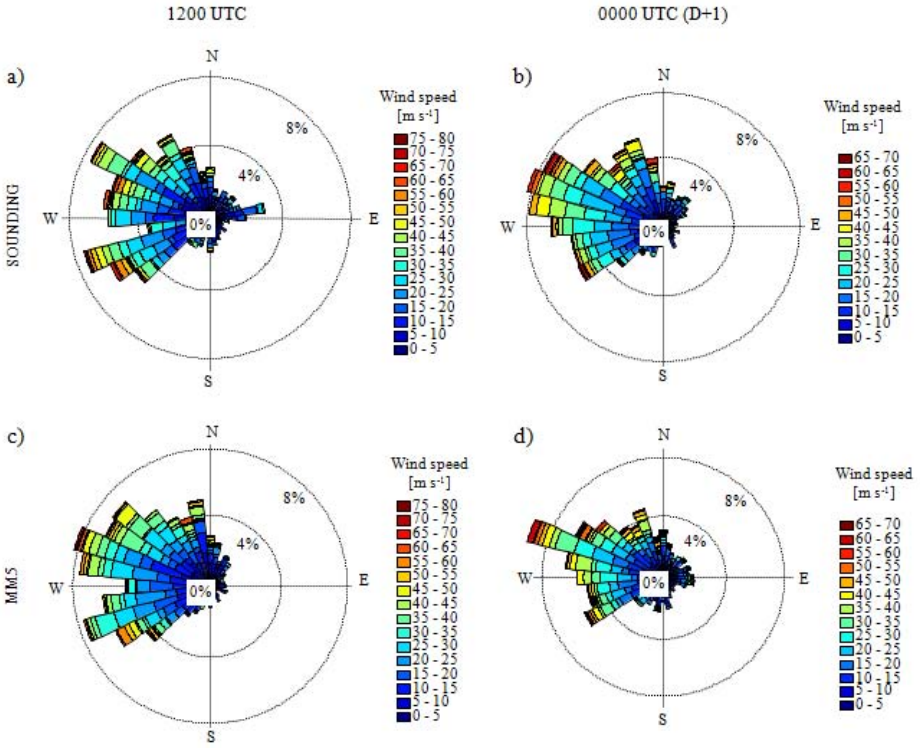

Figure 6: Top: Wind roses indicating wind direction and speed at all levels according to the radiosonde (a) at 1200 UTC and (b) at 0000 UTC (D+1). Bottom: Wind roses indicating wind direction and speed at all levels according to the MM5 (c) at 1200 UTC and (d) at 0000 UTC (D+1).

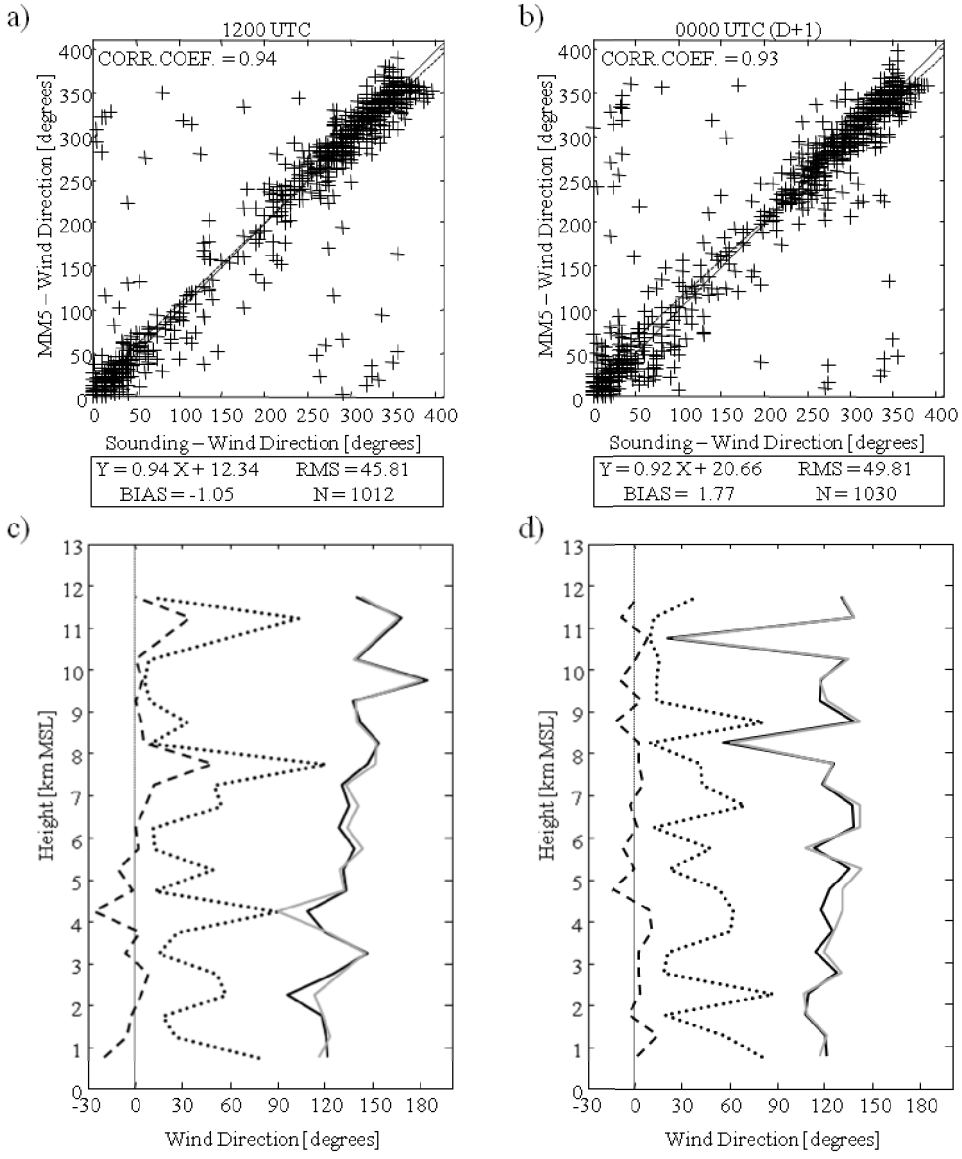

Figure 7: The same as Fig. 2, but for wind direction.

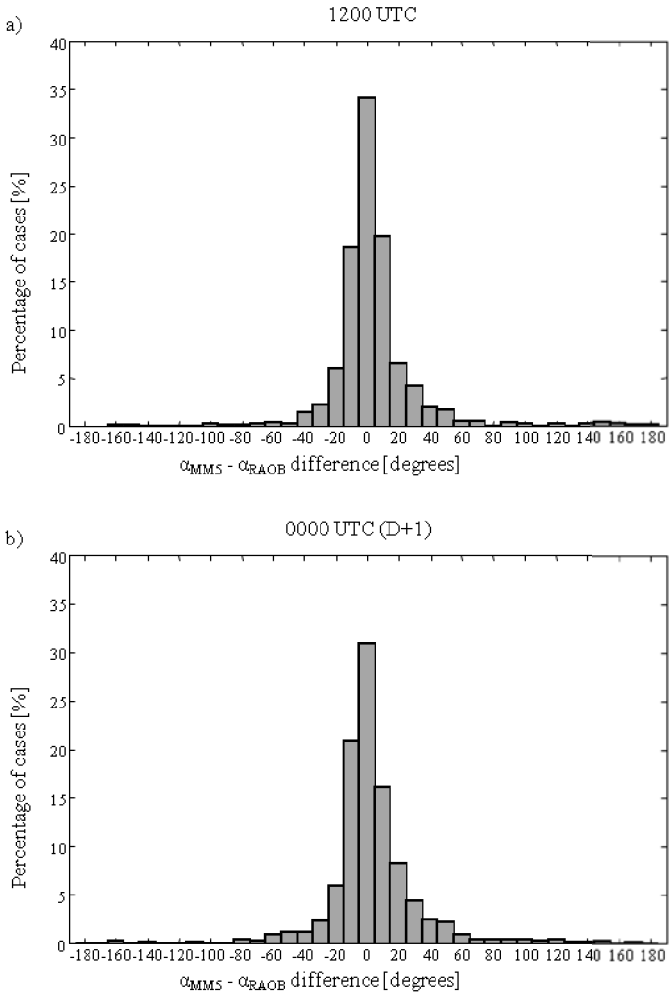

Figure 8: Histograms of angle differences (α_{RW}-α_{MM5}) in decimal degrees (a) at 1200 UTC and (b) at 0000 UTC (D+1).